Upscreening of NVE IL611 Digital Isolator

Sedlmayr, Hans-Jürgen and Hacker, Franz and Kunze, Klaus and Maier, Maximilian

The Compliant Assistance and Exploration SpAce Robot (CAESAR) is the space qualified equivalent to the current service robot systems for manufacturing and human-robot cooperation. It was developed by the Institute of Robotics and Mechatronics at the German Aerospace Center (DLR) and is designed for a variety of on-orbit services e.g. assembly, maintenance, repair, and debris removal in LEO/GEO. It is used within the European Robotic Orbital Support Services In Orbit Demonstrator (EROSS IOD) mission. Crucial for the operation of the robotic arm is the central power unit which have to fulfill multiple requirements of the robotic arm and of the spacecraft on the other hand. Since the design of the Base Power and Isolation Unti (BPIU) is such, that the primary power domain of the Spacecraft is galvanically isolated from the secondary power domain, digital signals e.g. for retrieving housekeeping information have to be routed through this isolation barrier which requires digital isolators. These parts are able to withstand a voltage difference between both power domains and transmit a digital signal from one domain to the other. Within the current BPIU design, the tested digital isolator IL611 from NVE shall be used for this task. Therefore, the part was screened for Total Ionizing Dose (TID) initially. Afterwards a Proton Test and a Heavy Ion Test were conducted. This paper highlights the most important results of the conducted tests.

Sedlmayr, Hans-Jürgen and Hacker, Franz and Kunze, Klaus and Maier, Maximilian (2024) Upscreening of NVE IL611 Digital Isolator. In: 2024 RADECS Data Workshop. RADECS Conference, 16.09.2024 - 20.09.2024, Maspalomas, Canary Islands, Spain

Up-screening of NVE IL611 Digital Isolator

Hans-Juergen Sedlmayr[1] and Franz Hacker[1] and Klaus Kunze[1] and Maximilian Maier[1]

***Abstract*—The Compliant Assistance and Exploration SpAce Robot (CAESAR) is the space qualified equivalent to the current service robot systems for manufacturing and human-robot co-operation. It was developed by the Institute of Robotics and Mechatronics at the German Aerospace Center (DLR) and is designed for a variety of on-orbit services e.g. assembly, maintenance, repair, and debris removal in LEO/GEO. It is used within the European Robotic Orbital Support Services In Orbit Demonstrator (EROSS IOD) mission. Crucial for the operation of the robotic arm is the central power unit which have to fulfill multiple requirements of the robotic arm and of the spacecraft on the other hand. Since the design of the Base Power and Isolation Unti (BPIU) is such, that the primary power domain of the Spacecraft is galvanically isolated from the secondary power domain, digital signals e.g. for retrieving housekeeping information have to be routed through this isolation barrier which requires digital isolators. These parts are able to withstand a voltage difference between both power domains and transmit a digital signal from one domain to the other. Within the current BPIU design, the tested digital isolator IL611 from NVE shall be used for this task. Therefore, the part was screened for Total Ionizing Dose (TID) initially. Afterwards a Proton Test and a Heavy Ion Test were conducted. This paper highlights the most important results of the conducted tests.**

***Index Terms*—Digital Isolator, On Orbit Servicing, Power Supply, Space Robotics, Up-screening**

I. Introduction

THE increasing number of used robotic systems in space and the expected increasing demand of robotic systems shows that robotic manipulators play an important role in space exploration and pave the way for satellite lifetime extensions, orbital asset inspections, and deorbiting. CAESAR [1] is designed for a variety of on-orbit services e.g. assembly, maintenance, repair, and debris removal in LEO/GEO and is used within the EROSS IOD mission [2]. This EU-funded project aims to demonstrate autonomous tasks for On-Orbit Servicing (OOS), including rendezvous, refuelling and replacement of components, which will help to maintain and extend the client satellite's lifespan. Within this mission multiple servicing tasks based on one servicing satellite and one client satellite, that has to be serviced, are planned. Fig. 1 shows the CAESAR arm in the lab, which is supported by a Motion Suspension Systems.

A reliable operation of the CAESAR arm strongly depends on a reliable power supply. This includes that the power supply protects the robotic arm, the satellite and itself from overload or voltage transients. Therefore, the design of the BPIU is such, that the primary power domain of the Spacecraft is galvanically isolated from the secondary power domain. In consequence of the isolation, digital signals for control and monitoring have to be routed through this galvanic barrier. For example the housekeeping data can be read by means of a differential Serial Peripheral Interface (SPI) which could be connected to the relevant control system. More details on the BPIU design can be found at [3].

Fig. 1. *CAESAR robotic arm, supported by a Motion Suspension System, Credits [3], Copyright © 2023, IEEE*

When digital signals have to be transmitted over a galvanically isolation, so called digital isolators are used. These parts are able to withstand a voltage difference between both power domains, provide the needed isolation of both sides, transmit the input signal from one domain to the other and are capable of adopting the signals to different signal levels in both power domains. In modern system designs, where an increasing number of signals from different power domains and with different voltage levels (e.g. dig I/O signal at modern FPGAs vs. sensor signals) have to be tied together, these parts are getting more and more important.

There are multiple options to transfer digital signals over a galvanically isolation. At the moment, the most common ones are optocouplers. Since there are different topologies on the market, a general reference of the radiation performance of optocouplers is not available. The total ionizing dose response of a few samples for usage in space reach from 100 Gy (10 kRad) up to 2000 Gy (200 kRad, non-exhaustive list).

Furthermore, some optocouplers have a rather high current consumption and a rather large package. Both disadvantages are the reasons, why non optical isolators were investigated more in detail.

One of the multiple possibilities is the IL611 from NVE which utilizes NVE's patented IsoLoop® spintronic Giant Magnetoresistive (GMR) technology [4]. This technology guarantees a small form factor, high speed and low power consumption according to the manufacturer.

In addition to the current test campaign, multiple commercial non-opto galvanic isolators have already been tested [5].

[1]These authors are with the Robotics and Mechatronic Center, DLR, Oberpfaffenhofen, Germany; Contact: hans-juergen.sedlmayr@dlr.de

II. Device Description

The isolator family IL600 from NVE offers multiple parts with different channel numbers in multiple configurations. The investigated part IL611 is able to transmit two unidirectional digital signals. A functional diagram of the IL611 is shown in Fig. 2. The driver circuit contains a coil and the produced magnetic field modifies the resistance of the GMR layered structures which changes the output voltage.

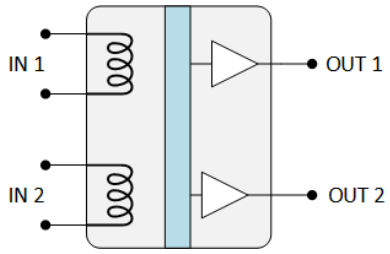

Fig. 2. *Functional diagram of the NVE IL611*

At the IL611 input stage both sides of the coil are accessible, which enables the possibility of an inverting or non-inverting transmission. The device is available in a 8-pin MSOP, a 8-pin SOIC and a 8-pin PDIP package. For our tests we used parts with the 8-pin SOIC package.

The recommended supply voltage range of the device is 3.0V up to 5.5V and the recommended temperature range is -40 °C up to +100 °C. In our applications the part is used with a supply voltage of 3.3V only, therefore, the supply voltage was set to 3.3V during the tests.

III. Environment

The radiation requirements for the EROSS IOD mission stipulate that the used parts shall not exhibit destructive Single Event Effects (SEE) like Single Event Latchup (SEL) below 15 MeV·cm^2/mg and no non-destructive SEE below 0.4 MeV·cm^2/mg. The TID limit was defined at 100 Gy (10 kRad) for the mission.

The temperature of the CAESAR electronics ranges from -30 °C up to +60 °C during the EROSS IOD mission. This is in line with the recommended temperature range of the device.

IV. Radiation Tests

A. Overview

In order to have an upper limit of the TID resilience of the IL611 for the upcoming particle tests, a TID test using gamma rays at HZB's Co^{60} cell [6] was conducted with a dose rate of 12.6 Gy/h (1.26 kRad/h, ESCC standard rate). Afterwards a proton test was performed in air and at room temperature at HZB's proton therapy accelerator [6] with following parameters:

- Flux: 2.0 · 10^7 Protons / (cm^2·s)
- Fluence: 2.0 · 10^{10} Protons / cm^2
- Proton Energies: 68, 50 and 30 MeV

A heavy ion test campaign was also performed at the RADEF (RADiation Effects Facility, [7]). The test was conducted in air and at room temperature with the rated supply voltage. For the irradiation the 16.3 MeV/u cocktail of the test facility was used. All devices were delidded by chemical etching.

Table I shows the used ion species, the applied tilt angle and the effective LET. A tilt angle of 0 degree is the normal incidence of the beam. To increase the effective LET, some of the measurements were done with an angle of incidence up to 50 degrees, which gave a maximum effective LET of 97.2 MeV·cm^2/mg. The applied fluence of 1.0 · 10^7 ions per square centimeter was used for each ion species.

TABLE I
Used ion species and their LET values

section	ion species	tilt-angle $[degree]$	effective LET $[MeV \cdot cm^2/mg]$
1	$^{20}Ne^{7+}$	45	3.3
2	$^{57}Fe^{20+}$	45	22.6
3	$^{83}Kr^{29+}$	0	31.0
4	$^{83}Kr^{29+}$	45	43.8
5	$^{107}Ag^{37+}$	35	61.0
6	$^{107}Ag^{37+}$	50	77.8
7	$^{126}Xe^{44+}$	45	88.4
8	$^{126}Xe^{44+}$	50	97.2

B. Test setup

A functional diagram of the test configuration of the IL611 is shown in Fig. 3. This setup was used for all three test campaigns. The DUT (Device Under Test) is connected to the interface board of the RTM (Radiation Test Motherboard) which provides the interface to the control and data logging PC in the control room. In particular all digital I/O-lines and the power supply line are routed to the DUT. Since the I/O voltage of the DSP on the RTM is compatible with the DUT, the Interface board contains no additional logic.

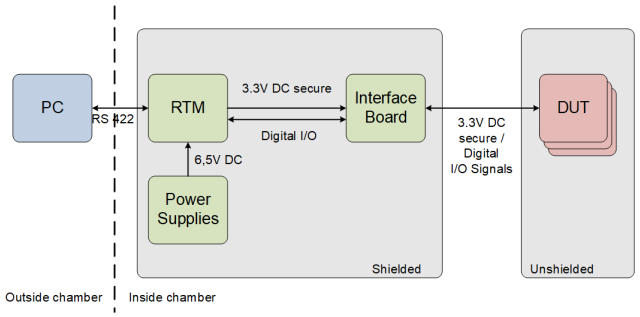

Fig. 3. *NVE IL611 test configuration*

The RTM itself contains some circuitry which monitors and measures up to 6 power supply lines with up to 1A and up to 6.5V each. The monitoring realizes a latch-up protection with an adaptive alert threshold level which interrupts the power supply and short circuits the power line by means of a crow bar when the supply current is above the limit. This is indicated by the phrase "3.3V DC secure" in Fig. 3.

Also, the DSP on the RTM controls the test sequence, measures the supply current, provides the input signals of the DUT (test stimuli) and reads the output signals of the DUT (DUT answer). Finally, after each complete cycle the collected data are sent to the control PC. Fig. 4 shows a rough overview of the test sequence. After the RTM is configured to operate in the wished state, the DUT is powered and the test sequence which consists of the four orange steps is processed until an error occurs (e.g. Latch-up) or the user sends a stop command from the control PC. Both will clear the ”continue test” - flag and afterwards the RTM return to idle mode after the power of the DUT is switched off.

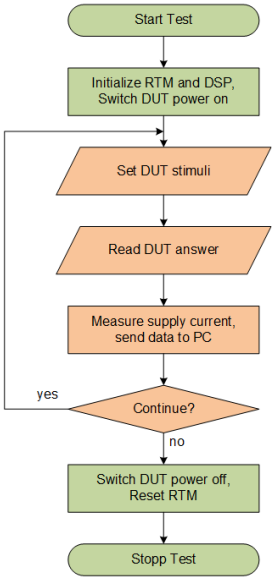

Fig. 4. *NVE IL611 test sequence*

During the test campaigns the IL611 is operated in an inverting single ended configuration. This means, that the signal of the driving DSP will be read out from the IL611 with an inverted level at the corresponding output. During the test both input ports of the DUT were driven in all four possible configurations in cyclic order (0-0, 0-1, 1-0, 1-1) to detect possible cross coupling effects. Each time, when a new stimuli configuration is asserted by the control DSP, the outputs of the DUT were recorded together with the corresponding stimuli. This data set is recorded by the control DSP and finally transmitted by a serial interface to the control and data logging PC. Fig. 5 shows the principle of the measurement.

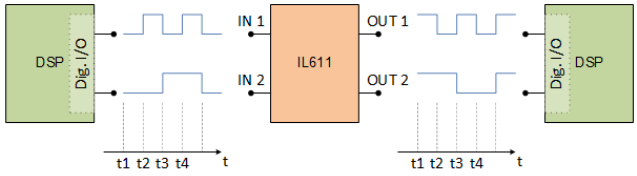

Fig. 5. *NVE IL611 principle of measurement*

For the proton and the heavy ion tests, the same setup was used. But instead of reading one set of data within 5 seconds, 2 values per second were recorded during the particle tests to detect short term events based on the irradiation.

During the subsequent offline analysis, the difference between input and output of each channel was calculated which shall be zero when the device works properly. The inversion of the signal was already compensated during the recording of the data. Equation (1) shows the performed calculation.

$$\Delta_m[n] = x_m[n] - y_m[n] \tag{1}$$

Whereby $y_m[n]$ is the sampled output signal of the IL611 (values: 0 or 1) and $x_m[n]$ is the corresponding input signal of the DSP (values: 0 or 1). The subscript ’m’ indicates the configuration of the input signals (range: 0 up to 3). Finally, the index n defines the record number.

Table II shows the expected values of the performed calculation. Please notice that the value ’-1’ is a valid result of the calculation which indicates an error.

TABLE II
Expected values of the data analysis

$x_m[n]$	$y_m[n]$	$\Delta_m[n]$	Result
0	0	0	ok
0	1	-1	*failure*
1	0	1	*failure*
1	1	0	ok

Finally, due to the fact that $\Delta_m[n]$ is not equal zero in case of functional errors and equal zero for a properly working device, errors can be found very easily. During all three test campaigns a device was treated as ”non-operational” when at least one output signal hasn’t changed its polarity for more then 10 cycles.

V. TID Test

The test setup of the TID test is shown in Fig. 6. Three test boards were used, whereby each test board contains one isolator with two channels. They were placed in a circle around the Co60 source with an equalized distance.

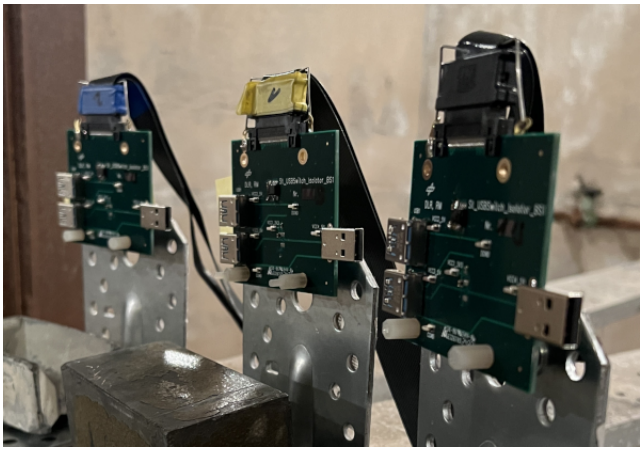

Fig. 6. *Test setup in the TID Chamber*

The irradiation was stopped at a TID level of 1629 Gy(Si) (162.9 kRad(Si)). Up till 1165 Gy(Si) (116.5 kRad(Si)) we found all six Channels working. At this dose level, the first channel of the second DUT stopped bit by bit its operation. Later on, at 1415 Gy(Si) (141.5 kRad(Si)) the second channel of the third DUT stopped its operation. Both affected output signals stuck at zero. At the end of the test, 4 channels splitted over all three devices still were working.

A. Test Results

As already described in the last chapter the difference between the input and the output is a good indicator for a working device. Fig. 7 shows the summary of all six channels after the data were processed with Equation 1. The y-Axis shows the results in increments and the x-Axis the applied dose level in Gy(Si). The label 'Board' corresponds to the DUT number with its two channels. Clearly visible are both failing channels where the difference between the input and the output is not zero.

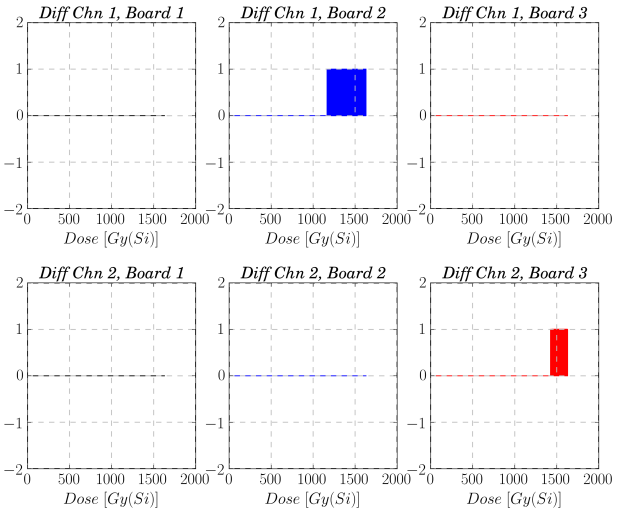

Fig. 7. *Summary of the TID test campaign*

Fig. 8 and Fig. 9 show the failures of the damaged channels more in detail. In both figures the upper sub-figure shows the recorded raw data of the channel over dose, while the lower sub-figure displays the result of the calculated difference over dose. It's obvious that the output stage stopped its operation and the output level remained stuck at '0'. Due to the limited resolution of the plots, single transitions of the output signal at the end of the working phase or corresponding single transition failures may not be visible.

During the whole TID test the supply current was within the rated limits, therefore it is not plotted here.

B. Annealing

Immediately following the return from Berlin, a high temperature annealing at 100 °C was initiated. After 28 hours of annealing, every device was working properly again without measurable degradation. Therefore, the annealing was stopped two hours later.

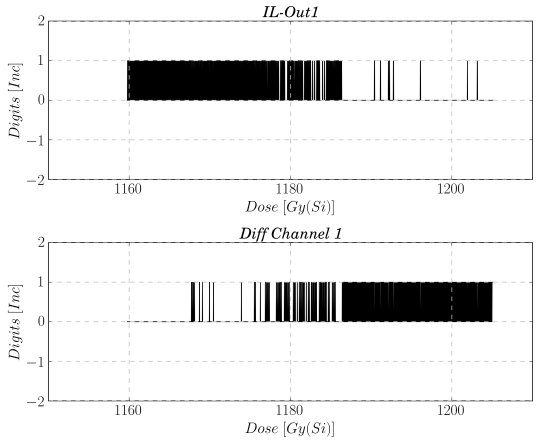

Fig. 8. *Board Number 2 Failure*

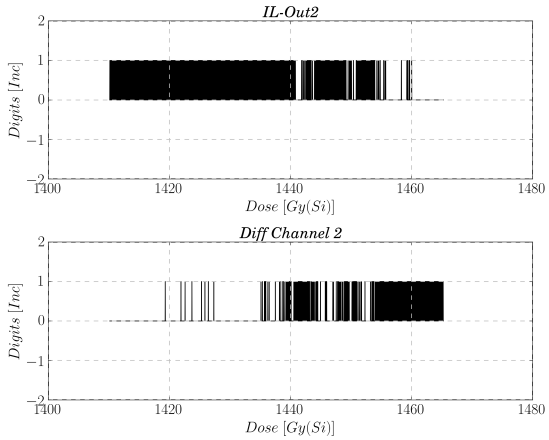

Fig. 9. *Board Number 3 Failure*

Fig. 10 shows the summary of the annealing measurements of all six channels after the data were processed with Equation 1, similar to Fig. 7. The y-Axis shows the results in increments and the x-Axis the measurement time in seconds. The label 'Board' corresponds to the DUT number with its two channels.

In order to have a compact plot, the test results in Fig. 10 are displayed in a condensed way. Every third shows a snipped of 3 hours of measurement, starting at different times during the annealing process. The first third shows the results of the first three hours of the annealing procedure. The middle third (starting with the red dotted line) shows the results after 3.5 hours of annealing. Finally, the last third (starting with the green dotted line) shows the results after 27 hours of annealing, where both channels returned to normal operation which is indicated by the zero as a result of processing the data with Equation 1.

Fig. 11 and Fig. 12 show the return to normal operation more in detail. In both figures the upper sub-figure shows the recorded raw data of the channel, while the lower sub-figure displays the result of the calculated difference. Contrary to Fig. 10, are samples plotted on the x-axis, that means every data point represents 3 seconds of testing time.

Similar to the failure mechanism but in opposite direction,

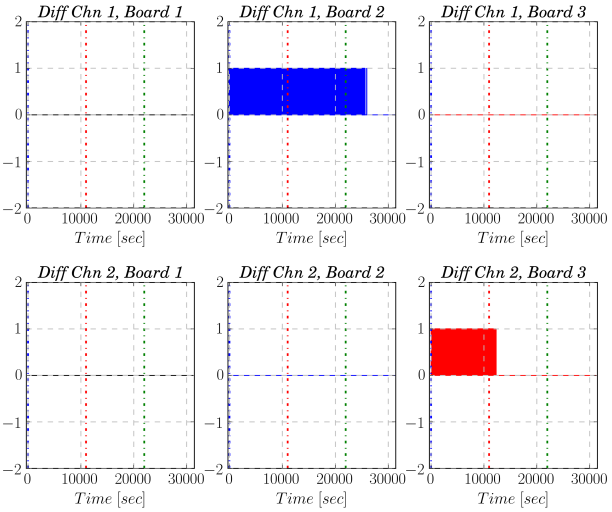

Fig. 10. *Summary of the annealing process*

the driver stage started to operate temporarily after a while and finally it returned to normal operation. This is indicated by the alternating output signal in the upper sub-figures and the difference of zero in the lower sub-figures. Due to the limited resolution of the plots, single transitions of the output signal at the begin of the working phase may not be visible.

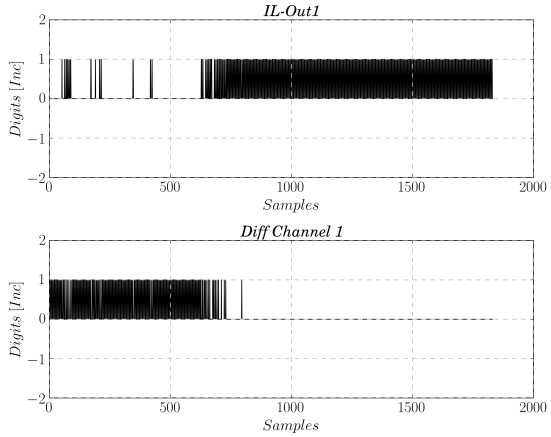

Fig. 11. *Return to normal operation of Board Number 2*

VI. Proton Test Results

During the proton test campaign no serious error was measured. Also, the supply currents were within the rated limits during the whole irradiation and no upsets were detected. Fig. 13 shows one device during the beam positioning procedure before the irradiation. The red cross on the device marks the beam location.

Similar to the plots in the previous sections, the difference between input and output signal is plotted in Fig. 14. However, contrary to the dose information, the beam time is used as x-axis. In order to have a compact plot, all test sections with the different particle energies are concatenated. The start of each section is indicated by a colored vertical dotted line. These

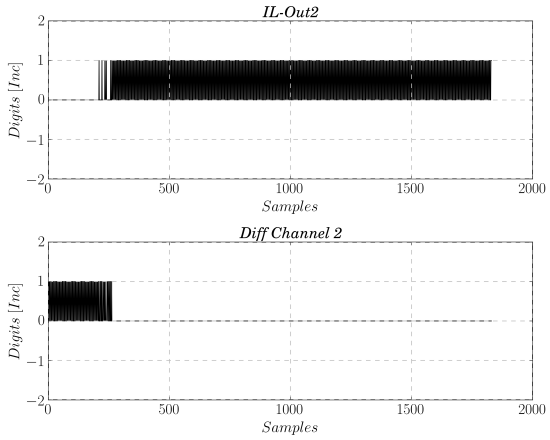

Fig. 12. *Return to normal operation of Board Number 3*

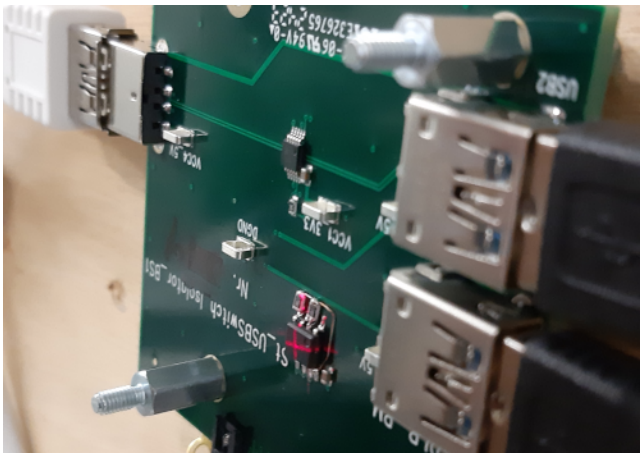

Fig. 13. *Beam positioning at HZB proton facility*

sections correspond to the proton energies: 68 MeV (section I); 50 MeV (section II); 30 MeV (section III). As expected, the differences between the input level and the output level are zero, which indicates a fully working device. The label 'Board' corresponds to the DUT number with its two channels.

VII. Heavy Ions Test Results

No serious error was measured during the heavy ion test campaign. As listed in Table I, some of the measurements were done with a tilted device in order to increase the effective LET. Finally, the highest effective LET was 97.2 MeV·cm^2/mg which was achieved during a test run with Xe ions and an applied tilt angle of 50°.

Fig. 15 shows the test setup at the RADEF facility. Three test boards with one device on it were mounted in parallel on the universal test board mounting plate. Since the test was performed in air, the DUTS were positioned directly in front of the beam window before the irradiation was started.

Similar to the plots in the previous sections, the difference between input and output signal is plotted in Fig. 16 over the beam time which is used as x-axis. In order to have a compact plot, all test sections with the different particle energies are concatenated. The start of each section is indicated by a

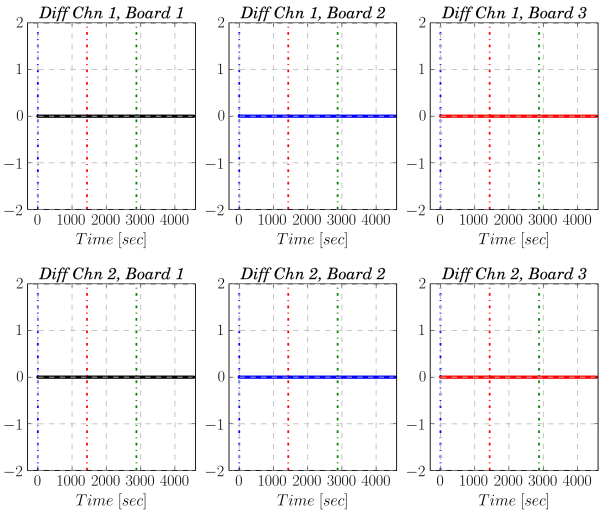

Fig. 14. *Summary of the Proton test campaign*

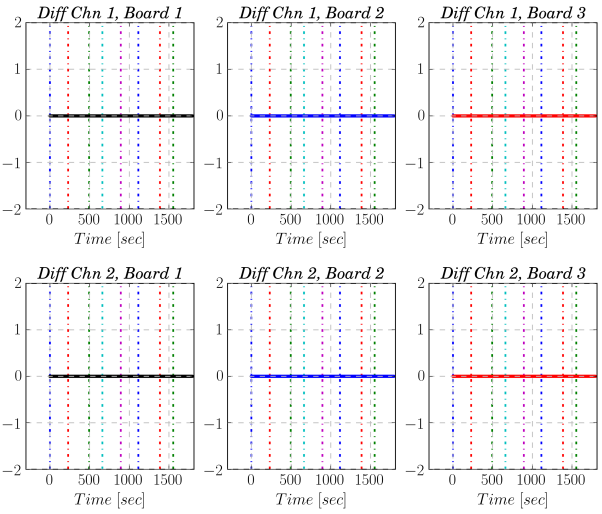

Fig. 16. *Summary of the heavy ion test campaign*

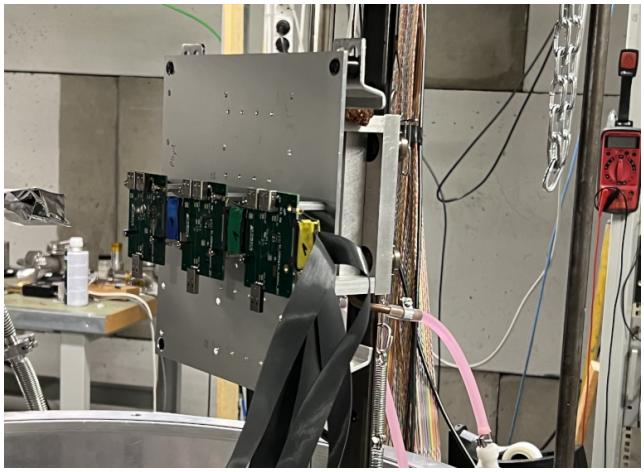

Fig. 15. *Test setup at RADEF facility*

colored vertical dotted line. These sections correspond to the ion species which are listed in Table I. For your convenience, the first column of Table I shows the section number which corresponds to the section in Fig. 16

As expected, the differences between the input level and the output level is zero, which indicates a fully working device. During the irradiation the supply current was measured, too. But similar to the proton test, no upsets or high current events were found. In addition, the current was within the rated limits during the whole test.

VIII. Conclusion

The tested galvanic digital isolator IL611 from NVE demonstrated a good resistance against SEL (Single Event Latchup) and SEE (Single Event Effects) during the tests with heavy ions and protons.

In addition, during the irradiation with the Co^{60} source up till 1165 Gy(Si) (116.5 kRad(Si)) no severe error was measured and the supply current was within the rated limits. After the devices stopped partly their operation due to the deposited TID at a level above 1165 Gy(Si) (116.5 kRad(Si)), they returned to normal operation after high temperature annealing.

The achieved results are in line with the test results which were presented at [5]. In summary, the results of the actual test campaigns make the NVE IL611 a promising flight candidate.

IX. Acknowledgement

This work was performed within the SpaceDream [8] and EROSS IOD [2] project framework and supported by multiple colleagues of the DLR Institute of Robotics and Mechatronics. The authors would like to thank them for their support.

References

[1] G. Grunwald, A. Beyer, M. Heumos, M. Schedl, R. Bayer, W. Bertleff, B. Brunner, R. Burger, J. Butterfass, R. Gruber, T. Gumpert, F. Hacker, E. Kraemer, M. Maier, S. Moser, J. Reill, M. Roa, H.-J. Sedlmayr, N. Seitz, M. Stelzer, A. Stemmer, G. TubioManteiga, T. Wimmer, M. Grebenstein, C. Ott, and A. Albu-Schaeffer, "CAESAR: Space Robotics Technology for Assembly, Maintenance, and Repair," in *69th International Astronautical Congress (IAC), Bremen, Germany, IAC-18,D1,6,3,x42634*, 2018.

[2] PIAP Space Sp. z o.o., "European Robotic Orbital Support Services," 2024, https://eross-h2020.eu/.

[3] S. Moser, A. Beyer, and F. Hacker, "Flexible Base Power and Isolation Unit for Robotic Payloads," in *13th European Space Power Conference (ESPC)*, 2023.

[4] NVE Corporation, "IL600 and IL600A Series Passive-Input Optocoupler Replacements," 2024, https://www.nve.com/il600.

[5] M. A. Jacobson, S. P. Buchner, H. L. Hughes, and P. J. McMarr, "SEE and TID Results for Commercial NonOptogalvanic Isolators for Space Application," in *IEEE Radiation Effects Data Workshop, 10.1109/REDW.2010.6062508*, 2011.

[6] (2024) Helmholtz Zentrum Berlin Wannsee, Cobalt-60-Source. [Online]. Available: https://www.helmholtz-berlin.de/forschung/oe/be/protonentherapie/index_de.html

[7] (2024) University of Jyvaskyla, Radiation Effects Facility - RADEF. [Online]. Available: https://www.jyu.fi/en/science/accelerator-laboratory/facilities-and-instruments/radiation-effects-facility

[8] M. Maier, M. Pfanne, H.-J. Sedlmayr, A. Kolb, M. Chalon, R. Bayer, W. Friedl, T. Wüsthoff, A. Meenakshi Sundaram, and M. Bihler, "TINA: The Modular Torque Controlled Robotic Arm - a Study for Mars Sample Return," in *2021 IEEE Aerospace Conference, BigSky, USA, doi: 10.1109/AERO50100.2021.9438222*, 2021.